Eur. Phys. J. D **44**, 439–447 (2007)
DOI: 10.1140/epjd/e2007-00219-1

THE EUROPEAN PHYSICAL JOURNAL D

Photoionization cross section and oscillator strength distribution in the near-threshold region of strontium

S.-U. Haq, S. Mahmood, M.A. Kalyar, M. Rafiq, R. Ali, and M.A. Baig[a]

Atomic and Molecular Physics Laboratory, Department of Physics, Quaid-i-Azam University, Islamabad 45320, Pakistan

Received 16 April 2007 / Received in final form 2 June 2007
Published online 29 June 2007 –

Abstract. We present experimentally measured absolute values of the photoionization cross sections from the $5s5p\ ^1P_1$ and $5s5p\ ^3P_1$ excited states of strontium at the first ionization threshold as 11.4 ± 1.8 Mb and 10.7 ± 1.7 Mb respectively using saturated absorption technique along with a thermionic diode ion detector in conjunction with a Nd:YAG pumped dye laser system. These threshold photoionization cross sections values have been utilized to determine the oscillator strengths of the $5s5p\ ^1P_1 \rightarrow 5snd\ ^1D_2$ and $5s5p\ ^3P_1 \rightarrow 5snd\ ^3D_2$ Rydberg transitions. The oscillator strength densities in the continuum corresponding to the $5s5p\ ^3P_1$ excited state have also been determined by measuring the photoionization cross sections at five ionizing wavelengths above the first ionization threshold. Smooth merging of the discrete f-values into the oscillator strength densities has been observed for the $5s5p\ ^3P_1 \rightarrow 5snd\ ^3D_2$ series across the ionization threshold.

PACS. 32.30.Jc Visible and ultraviolet spectra – 32.80.Dz Autoionization – 32.80.Fb Photoionization of atoms and ions – 32.70.Jz Line shapes, widths, and shifts

1 Introduction

The oscillator strength of a transition is proportional to the square of the dipole matrix element connecting two atomic or molecular states. The measurement of oscillator strength and that of photoionization cross section is a subject of considerable interest for many fields. It provides useful information about the strength of a transition and has significant importance in radiation physics, plasma physics, astrophysics and thermonuclear research. The oscillator strengths of atomic systems allow determination of the optical properties of atoms, transition rate for absorption, emission and lifetimes of the excited states. The distribution of the dipole oscillator strength as a function of excitation energy is an important property of atoms and molecules [1]. In the discrete region the oscillator strength directly determines the photoabsorption cross section whereas, in the continuum the distribution of the oscillator strengths yields the absolute value of the photoionization cross section and they merge smoothly from the discrete region into the continuum. Different experimental techniques have been used to determine the oscillator strength of a transition such as through emission, absorption or dispersion measurements or via combined measurements of branching ratio and lifetimes [2]. Huber and Sandeman [3] reviewed various techniques of oscillator strength measurements based on dispersion, absorption and emission and discussed merits and demerits of these techniques. The energy positions of the Rydberg states of strontium are well documented [4–11], but little data on oscillator strength is available in the literature as most of the available measuring methods have some limitations which restrict their range of applications. Wiese et al. [12] compiled the data on oscillator strengths of transitions and discussed various aspects of the methods used for these studies. Barrientos and Martin [13,14] applied the quantum defect orbital method to compute the oscillator strengths and the photoionization cross sections of the alkaline earth metals and obtained the oscillator strength distributions between the discrete and continuous spectra. Werij et al. [15] used a combination of the R-matrix, MQDT and modified Coulomb-approximation calculations along with the branching ratio measurements to get the transition rates for the allowed singlet and triplet transitions in strontium. Parkinson et al. [16] used the hook method to determine the f-values of the principal series of calcium, strontium and barium and extracted the photoionization cross section at the first ionization threshold from the oscillator strength distribution in the discrete and continuous spectra. Garton et al. [17] measured the relative f-values of the $5snp\ ^1P_1$ states using the magneto-optical rotation technique and compared their results with the earlier reported data. Mende and Kock [18] described

[a] e-mail: baig@qau.edu.pk

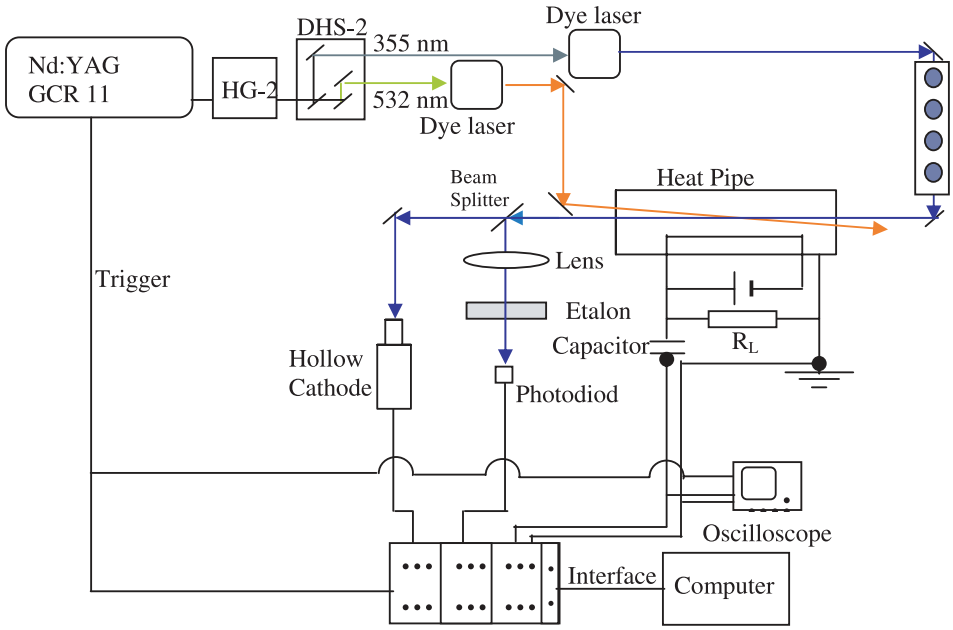

Fig. 1. A schematic diagram of experimental setup for the two-step photoionization studies of strontium.

an experimental technique to measure the absolute oscillator strengths of the Rydberg transitions of Sr and Ba using a thermionic diode ion detector. Absolute photoionization cross section was measured at the ionization threshold using the saturation technique [19–21], which was subsequently used to calibrate the f-values of the $5snp\ ^1P_1$ Rydberg transitions to put them on an absolute scale.

In the present work we have calibrated the f-values of the $5s5p\ ^{1,3}P_1 \rightarrow 5snd\ ^{1,3}D_2$, Rydberg series with the threshold photoionization cross sections measured from the $5s5p\ ^1P_1$ and $5s5p\ ^3P_1$ excited states of atomic strontium at the first ionization threshold using the saturated absorption technique. The photoionization cross sections above the first ionization threshold have also been measured and used to extract the oscillator strength densities in the continuum corresponding to the $5s5p\ ^3P_1$ excited state.

2 Experimental procedure

The experimental measurement of the oscillator strength of the $5s5p\ ^1P_1 \rightarrow 5snd\ ^1D_2$, and $5s5p\ ^3P_1 \rightarrow 5snd\ ^3D_2$ transitions of strontium have been conducted using the experimental arrangement shown in Figure 1. Thermionic diode is operated in the space charge limited mode and its working principle and linearity is well described [22,23]. This detector consists of a stainless steel tube 48 cm long, 3 cm diameter and1mm wall thickness. Both the ends are water-cooled and sealed with quartz windows. The tube was evacuated down to 10^{-6} Torr. The 20 cm central portion of the thermionic diode was heated by a clamp-shell furnace, operating at a temperature of ≈920 K corresponding to ≈0.2 Torr strontium vapor pressure [24]. The ultimate temperature was monitored by a Ni-Cr-Ni thermocouple and maintained within 1% by a temperature controller. A molybdenum wire of 0.25 mm diameter stretched along the tube was heated by a separate regulated power supply for the ion detection. About 5 g of strontium sample was placed in the central heating zone. Argon at a pressure of about 1 Torr was used as a buffer gas, which provided a uniform column of the strontium vapor and also protects the quartz windows from the chemical attack of the hot vapor. The ionization signal was optimized by adjusting the cathode current and the buffer gas pressure in the cell.

To measure the photoionization cross-section, the Hanna type dye laser [25] charged with Stilbene-420 dye pumped with the third harmonic (355 nm) of a Q-switched Nd: YAG laser (Spectra Physics, GCR-II) and tuned at 460.8 nm was used to populate the $5s5p\ ^1P_1$ excited state. These excited atoms were then ionized by the output of the second laser at threshold wavelength 412.6 nm. The ionization signals were registered as a change in the voltage across a 100 KΩ load resistor. The intensity of the ionizing laser was varied using neutral density filters (Edmund Optics) in the path of the ionizing laser beam and on each insertion, the energy was measured by an energy meter (R-752, Universal Radiometer) and the signal height was recorded on a storage oscilloscope. Similar steps were taken to record the photoionization data from the $5s5p\ ^3P_1$ excited state. The atoms were promoted to this excited state with a dye laser fixed at 689.4 nm. To measure the photoionization cross-section at threshold, the excited atoms were ionized with the second laser tuned at 318.2 nm. Besides we have measured the photoionization cross-section from the $5s5p\ ^3P_1$excited state above the ionization threshold at five ionizing wavelengths 317 nm, 315 nm, 313 nm, 310 nm and 266 nm.

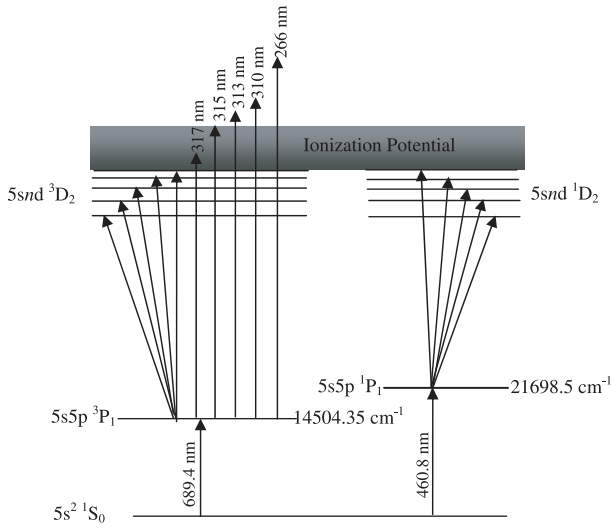

Fig. 2. A schematic energy level diagram of strontium showing the relevant levels in the excitation scheme. The level energies are taken from the NBS tables [42].

Following the excitation schemes shown in Figure 2, the $5s5p\ ^1\mathrm{P}_1 \rightarrow 5snd\ ^1\mathrm{D}_2$ ($19 \leqslant n \leqslant 68$) Rydberg series of atomic strontium have been recorded via the $5s5p\ ^1\mathrm{P}_1$ intermediate state. The scanning laser charged with Stilbene-420 dye and pumped by the third harmonic (355 nm) was scanned from 45550 cm^{-1} to 45960 cm^{-1}. Further more, we have recorded the $5s5p\ ^3\mathrm{P}_1 \rightarrow 5snd\ ^3\mathrm{D}_2$ ($24 \leqslant n \leqslant 70$) Rydberg series through the $5s5p\ ^3\mathrm{P}_1$ intermediate state. The dye laser, charged with DCM, dissolved in methanol and its frequency doubled output using BBO crystal was used to record the spectra covering the energy region from 45700 cm^{-1} to 45945 cm^{-1}. The wavelength calibrations during these experiments were achieved by recording simultaneously the output from the thermionic diode, the optogalvanic spectra of neon from a hollow cathode lamp and rings from a 1 mm thick fused silica Fabry-Perot etalon (FSR 3.33 cm^{-1}) via three boxcar averagers (SR 250). The optogalvanic signals from the neon hollow cathode lamp provided well distributed spectral lines of neon in the region of interest [26] that serve as wavelength standards. The interference fringes from the etalon were used to interpolate between the neon lines. The spectrum was recorded with a 0.05 cm^{-1} scanning step of the dye laser. From the location of the peak signal positions, the transition energies have been determined within an accuracy of ± 0.2 cm^{-1}.

In these experiments the dye laser pulse energy was $\approx$1 mJ and the line width of the dye laser was $\leqslant$0.3 cm^{-1}. The exciting and the ionizing laser beams were linearly polarized with parallel polarization vectors and passed through the thermionic diode from opposite sides and overlapped at its center. The temporal overlap of both the laser pulses was checked using a fast PIN photodiode (BPX 65). The relative delay between the exciting and the ionizing laser pulses was controlled and varied by an optical delay line.

3 Results and discussion

Strontium atom possesses two valence electrons outside a filled shell core with ground state electronic configuration as $5s^2\ ^1\mathrm{S}_0$. The odd parity $5snp\ ^1\mathrm{P}_1$ excited states can be approached via single photon excitation whereas the even parity $5sns\ ^1\mathrm{S}_0$ and $5snd\ ^1\mathrm{D}_2$ states can be accessed either via two-photon or through two-step excitation from the ground state. We have used a two-step excitation/ionization scheme for the measurement of the optical oscillator strength distribution in the discrete and continuous spectrum of strontium as shown in Figure 2.

The absolute oscillator strengths for the higher members of the $5s5p\ ^1\mathrm{P}_1 \rightarrow 5snd\ ^1\mathrm{D}_2$ and $5s5p\ ^3\mathrm{P}_1 \rightarrow 5snd\ ^3\mathrm{D}_2$ Rydberg series have been determined with the experimental technique developed by Mende and Kock [18]. A simple relation between the f-value of the Rydberg transition and the photoionization cross section measured at the ionization threshold is given as;

$$f_n = 3.77 \times 10^5 \frac{S_n\, \lambda_{1+}}{S_{1+}\, \lambda_n}\, \sigma^{1+}. \tag{1}$$

Here f_n is the oscillator strength for the nth transition of a Rydberg series, which is directly proportional to the photoionization cross section σ^{1+} measured at the threshold-ionizing wavelength λ_{1+}. The quantity S_{1+} is the ion signal at the ionization threshold and S_n is the integrated ion signal intensity for the nth transition.

As evident from the above equation, σ^{1+}, the absolute photoionization cross section at the ionization threshold is one of the essential parameter for the determination of the optical oscillator strengths of the Rydberg transitions. This absolute photoionization cross section from the $5s5p\ ^1\mathrm{P}_1$ and $5s5p\ ^3\mathrm{P}_1$ excited states at the first ionization threshold has been measured using the saturation technique [19,20]. This technique has been applied for the measurement of the photoionization cross sections from the excited states of alkali and alkaline earths ([19,20,27] and reference therein). This technique has been used to measure the photoionization cross sections and optical oscillator strengths of the auto-ionization resonances in neon [28] and photoionization cross sections of the excited states of helium and lithium [29,30].

The photo-ions produced as a result of excitation and subsequent ionization are detected in the form of voltage across the load resistor. The collected charge Q per pulse is represented as:

$$Q = \left(\frac{\mathit{Voltage\ signal}}{R}\right) \Delta t. \tag{2}$$

Here R is the load resistance and Δt is the pulse width of the photo-ion signal at FWHM.

In the absence of collisions and ignoring the spontaneous emission the solution of the rate equations for the two-step photoionization process, yields a relation between the total charge per pulse and absolute photoionization cross section [19,31] as;

$$Q = eN_{ex}\, V_{vol} \left[1 - \exp\left(-\frac{\sigma U}{2\hbar\omega A}\right)\right]. \tag{3}$$

Here e is the electronic charge, N_{ex} is the density of the excited atoms, A is the cross sectional area of the ionizing laser beam, U is the total energy per pulse of the ionizing laser, V_{vol} is the interaction volume and σ is the absolute photoionization cross section. This equation is valid under the assumptions that the intensity of the ionizing laser beam is much higher i.e. in access to that required for saturating the resonance transition, the transition remains saturated during the laser pulse and the laser beam is uniform and linearly polarized. The two-step photoionization depends upon the flux of the ionizing laser pulse, which enables the absolute measurement of the photoionization cross section. The accurate determination of the photoionization cross section σ requires accurate measurement of the ionizing laser energy as well as the characterization of the spatial profiles of both the exciting and the ionizing laser pulses in the interaction region. The uncertainty in the energy of the ionizing laser beam is mainly due to the fluctuations in the Nd:YAG laser, which is 5% and further 3%, is from the energy-measuring instrument. To characterize the exciting and the ionizing laser's spatial profiles, two beam splitters were placed before the entrance window of the thermionic diode and small fractions of the beams were used to observe the spatial profiles at the photon-atom interaction region. Both the exciting and the ionizing laser beams were scanned across the PIN photodiode and the spatial intensity profiles of both the laser beams were found to be of Gaussian distribution. Their spot sizes were determined at the point where the irradiance (intensity) falls to $1/e^2$ of their axial (peak) value. The exciting laser with a diameter ≈3 mm was passed through the center of the thermionic diode ion detector and the ionizing laser was first passed through the aperture to confine its diameter to ≈2 mm. This smaller diameter of the ionizer laser beam reduces the problems associated with the spatial overlap of the beams. A lens of 50 cm focal length was used in the path of the ionizing laser to meet the power requirements for saturation. The area of the overlap region in the confocal limit was calculated using the following relation [32,33]

$$A = \pi r_0^2 \left[1 + \left(\frac{\lambda_{io}\, l}{\pi r_0^2}\right)^2\right]. \qquad (4)$$

Here 'l' is the distance on the beam propagation axis from the focus ($l = 0$) and $r_0 = f\,\lambda_{io}/\pi\, r_s$ is the beam waist at $l = 0$, r_s is half the spot size of the ionizing laser beam on the focusing lens, f is the focal length and λ_{io} is the wavelength of the ionizing laser beam.

The linearity of the thermionic diode ion detector is very important while recording the experimental data of the photoionization signals so that an actual change of the photoions signal verses the energy density of the ionizing laser can be registered. We configured the linearity of our detector for the strongest photoion signal corresponding to the maximum available ionizing laser intensity. Collisional ionization due to the buffer gas atoms is the dominant process in a thermionic diode [23]. We have optimized the oven temperature and the buffer gas pressure such that the ionization probability for the observed Rydberg states

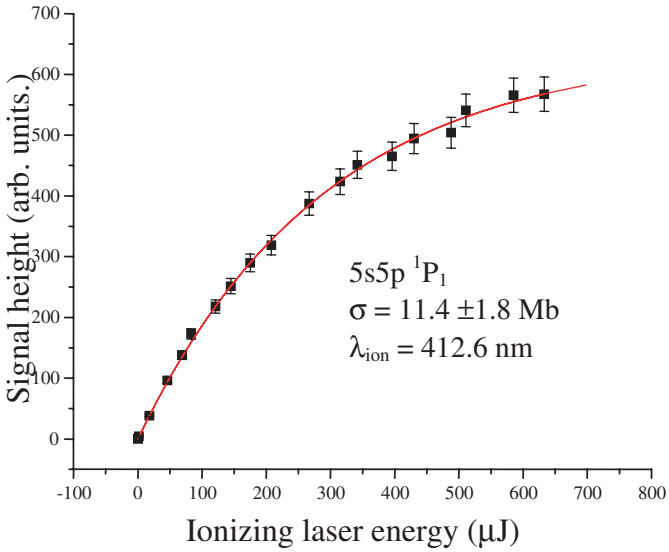

Fig. 3. The photoionization data form the $5s5p\ ^1P_1$ excited state to the first ionization limit. The solid line is the least squares fit of equation (3) to the observed data, to extract the photoionization cross-section σ (Mb) at the $5s$ thersold.

approaches to one [34], which is a necessary condition for using equation (1). Moreover, the energy difference between the lowest member of the observed Rydberg series and the ionization threshold is less than KT (0.08 eV at $T = 920$ K) for the present experimental conditions.

To measure the photoionization cross sections from the excited states at the first ionization threshold, the atoms were first excited from the ground state to the $5s5p\ ^1P_1$ and $5s5p\ ^3P_1$ states via single-photon absorption with the dye laser tuned at 460.8 nm and 689.4 nm respectively. In the second step the atoms were promoted to the ionization continuum by absorbing threshold wavelengths of 412.6 nm and 318.2 nm corresponding to the $5s5p\ ^1P_1$ and $5s5p\ ^3P_1$ excited states respectively. A typical data for the photoionization from the $5s5p\ ^1P_1$ state is shown in Figure 3. It is evident that as the laser intensity increases the ion signal rises up to a certain value very swiftly, then changes slowly and ultimately stops to increase further i.e. the signal gets saturated. The solid line, which passes through the experimental data points, is the least squares fit to equation (3). In Figure 4 we present two curves which are the fitted curves to the experimental data recorded at the threshold ionization wavelengths from the $5s5p\ ^1P_1$ and $5s5p\ ^3P_1$ excited states. The fitting procedure yields the photoionization cross section value at threshold as 11.4 ± 1.8 Mb from the $5s5p\ ^1P_1$ and 10.7 ± 1.7 Mb from the $5s5p\ ^3P_1$ state. Interestingly, the values of photoionization cross section from the $5s5p\ ^1P_1$ and $^3P_1$ states are very close in strontium. A 15% higher cross section from the triplet p-state as compared to that from the $6s6p$ P has been recently measured in barium. A factor of two difference has been theoretically predicted for $6s6p\ ^3P$ in ytterbium [35].

The photoionization cross section from the ground state to the first ionization threshold is well studied

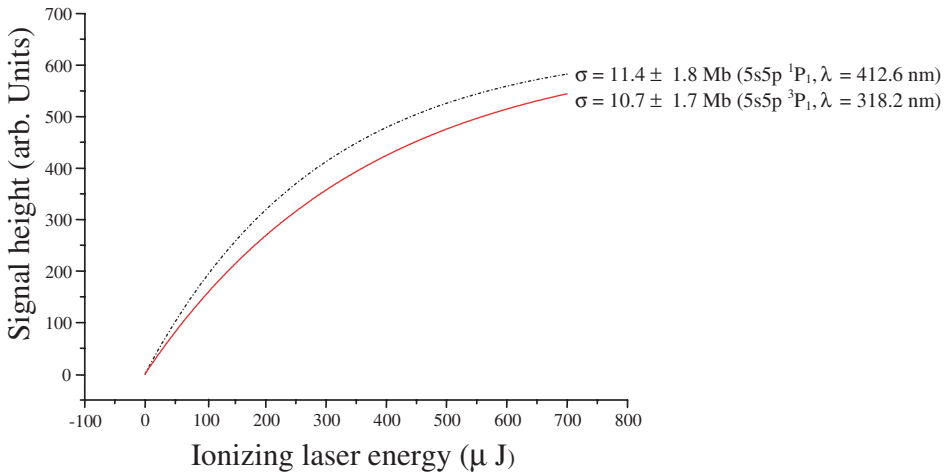

Fig. 4. Fitted curves to the experimental data for the photoionization cross-section from the $5s5p$ $^{1,3}P_1$ states of strontium at thershold.

[14,16,17,22,36]. Recently, Yih et al. [37] reported the photoionization cross section of strontium and also listed the earlier experimental and theoretical values at the $5s$ threshold ranging from 3 Mb to 13 Mb. Mende and Kock [18] determined the cross section from the $5s5p$ $^1P_1$ excited state of strontium at the first ionization threshold. Our measured value of the cross section from this excited state is 11.4 ± 1.8 Mb. To our knowledge no experimental as well as theoretical data of the photoionization cross section from the $5s5p$ $^3P_1$ excited states is available in the literature. These measured values of the photoionization cross section from the ^1P and ^3P excited states corresponding to the ionization threshold are used to extract the f-values of the above-mentioned Rydberg series.

Moreover, we have measured the photoionization cross sections from the $5s5p$ $^3P_1$ excited state above threshold at five ionizing laser wavelengths of 317 nm, 315 nm, 313 nm, 310 nm and 266 nm. Figure 5 shows the fitted curves for the photoionization cross sections from the $5s5p$ $^3P_1$ excited state at six different ionizing laser wavelengths. The measured values of the photoionization cross sections from this fitting procedure are 10.7 ± 1.7 Mb, 11.2 ± 1.7 Mb, 10.6 ± 1.7 Mb, 9.2 ± 1.5 Mb, 7.2 ± 1.1 Mb and 2.4 ± 0.38 Mb corresponding to the excess photon energies of 0 eV, 0.014 eV, 0.035 eV, 0.064 eV, 0.103 eV and 0.764 eV respectively. The extracted values of the cross section are given in Table 2 and are plotted against the excess photon energy in Figure 6. The measured photoionization cross section above the ionization threshold decrease smoothly from the 11.1 Mb at excess energy of 0.014 eV down to 2.4 Mb at 0.764 eV excess energy. This kind of decreasing trend of photoionization cross section is reported by Yih et al. [37] and Chu et al. [38] of the ground state. More recently, Martin and Hugo [39] calculated the single photon photoionization cross section between the $5s$ and $4d$ threshold, showing the smooth decrease in cross section near-above the $5s$ threshold. From the $5s5p$ $^3P_1$ excited state there is only one experimentally determined photoionization cross section at excess energy of 0.764 eV (at 266 nm) by Jones et al. [40] as 2.3 Mb. Our measured value at this excess energy is 2.4 ± 0.38 Mb which is in excellent agreement with that of Jones et al. [40].

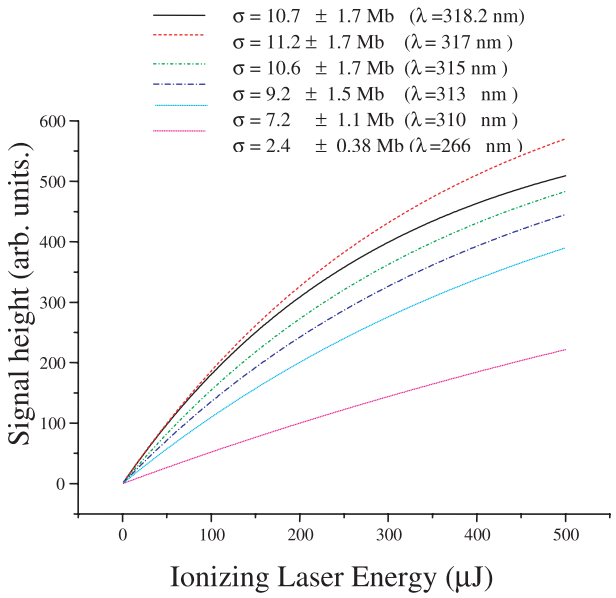

Fig. 5. The fitted curves to the experimental data verses the energy of the ionizing laser for the photoionization cross section from the $5s5p$ $^3P_1$ excited state of strontium at threshold (318.2 nm), 317 nm, 315 nm, 313 nm, 310 nm and 266 nm. The extracted photoionization cross-sections from the $5s5p$ $^3P_1$ excited state at these ionizing laser wavelengths are also shown.

In order to find the values of the remaining parameters λ_n, λ_{1+}, S_{1+} and S_n used in equation (1), we have recorded the Rydberg series $5s5p$ $^1P_1 \rightarrow 5snd$ $^1D_2$ and $5s5p$ $^3P_1 \rightarrow 5snd$ $^3D_2$ of strontium. Small portions of each of the recorded Rydberg series are shown in Figures 7a, 7b. The $5s5p$ $^1P_1 \rightarrow 5snd$ $^1D_2$ ($19 \leqslant n \leqslant 68$) Rydberg series have been recorded using $5s5p$ $^1P_1$ as an intermediate state covering the energy region from 45550 cm^{-1} to 45960 cm^{-1} is shown in Figure 7a. The intensities of the high members of the series decrease monotonically and the last observed Rydberg state $5s68d$ $^1D_2$ lies ≈25 cm^{-1} below the ionization limit. The $5sns$ $^1S_0$ series is also allowed but it is too weak to be detected in the present work. Esherick [5] reported the $5snd$ $^1D_2$

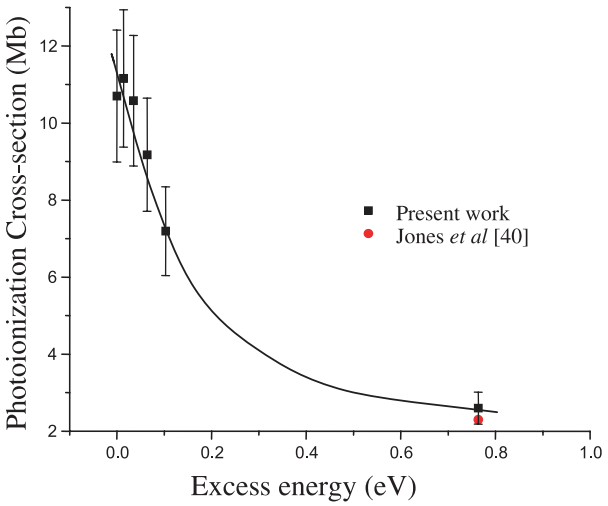

Fig. 6. A plot of the photoionization cross section verses the excess energy (above threshold) from the $5s5p\ ^3P_1$ excited state. The circular data point at excess energy 0.76 eV is the photoionization cross section measured by Jones et al. [40].

series ($5 \leqslant n \leqslant 60$) and Baig et al. [10] investigated the even parity $5s5p\ ^1P_1 \rightarrow 5snd\ ^{1,3}D_2$ Rydberg series using molecular dissociative sequential excitation and ionization. In Figure 7b, we have reproduced the Rydberg states excited from the $5s5p\ ^3P_1$ intermediate state. Two series are evident, the dominating series $5snd\ ^3D_2$ have been resolved up to $n = 70$ whereas the weak accompanied series, identified as $5sns\ ^3S_1$, is resolved from the $5snd\ ^3D_2$ series up to $n = 38$. However the dominating series is $5snd\ ^3D_2$, which is due to the larger spatial overlapping of the wave functions of the lower state to that of the excited nd than the ns states, which leads to higher transition amplitudes. This Rydberg series was reported by Esherick [5] ($5 \leqslant n \leqslant 37$) and Makdisi et al. [11] ($25 \leqslant n \leqslant 47$). The effective quantum number n^* have been calculated by using the Rydberg relation;

$$n^* = \sqrt{\frac{R_{\mathrm{Sr}}}{IP - E_n}} \tag{5}$$

where R_{Sr} is the mass corrected Rydberg constant of strontium 109736.6 cm^{-1}, E_n is the energy of the observed transition and IP is the ionization potential as 45932.09 cm^{-1} [26].

The absolute oscillator strength data for the $5s5p\ ^1P_1 \rightarrow 5snd\ ^1D_2$ and $5s5p\ ^3P_1 \rightarrow 5snd\ ^3D_2$ Rydberg series were then evaluated with the help of equation (1). The f-values of the $5s5p\ ^1P_1 \rightarrow 5snd\ ^1D_2$ transitions were calibrated with the threshold photoionization cross section (11.4 ± 1.8 Mb) corresponding to excitation from the $5s5p\ ^1P_1$ state. The measured f-values for the above-mentioned Rydberg series along with the principal quantum number (n), the wavelengths of the corresponding transitions and the earlier reported data [18] are listed in Table 1. The measured f-values of the $5s5p\ ^1P_1 \rightarrow 5snd\ ^1D_2$ Rydberg transitions along with those by Mende and Kock [18] for the same series are plotted against the principal quantum

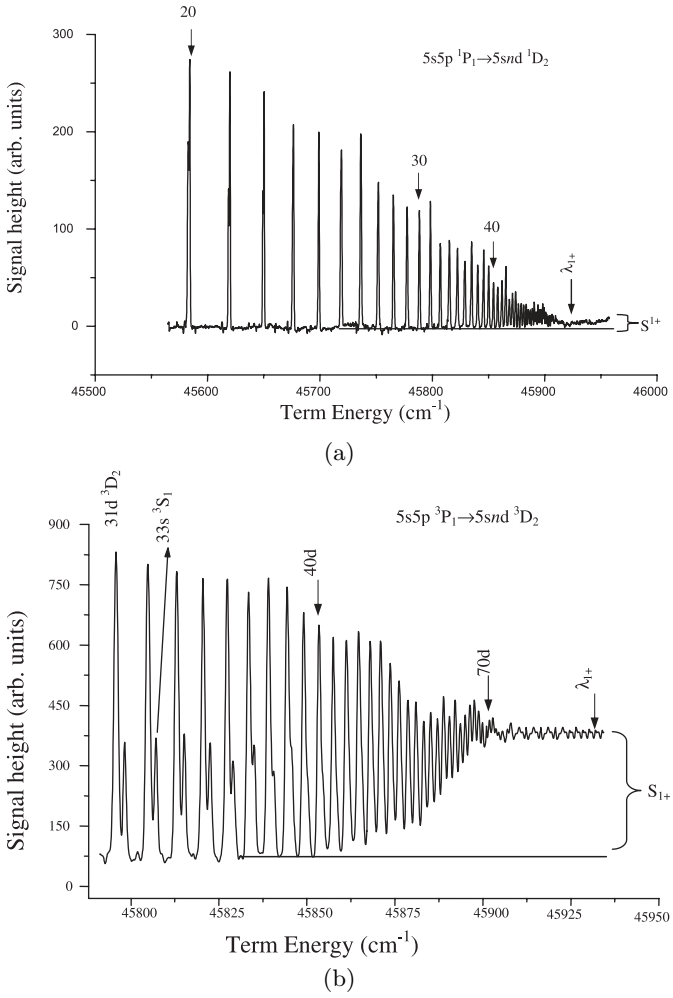

Fig. 7. (a) The $5snd\ ^1D_2$ ($19 \leqslant n \leqslant 68$) Rydberg states of strontium observed from the $5s5p\ ^1P_1$ excited level covering the spectral region between 45500–46000 cm^{-1}. (b) The $5snd\ ^3D_2$ ($24 \leqslant n \leqslant 70$) Rydberg states of strontium observed from the $5s5p\ ^3P_1$excited level covering the spectral region between 45750–45950 cm^{-1}.

number in Figure 8. Our measured values are in good agreement to those by Mende and Kock [18] within the experimental uncertainty. Moreover we have extended the oscillator strengths data towards the higher excited states ($19 \leqslant n \leqslant 68$). The product $n^{*3}f$ versus the principal quantum number (n) is shown in Figure 9 reflecting an increasing behavior.

Similarly the f-values of the $5s5p\ ^3P_1 \rightarrow 5snd\ ^3D_2$ ($24 \leqslant n \leqslant 70$) Rydberg transitions have been calibrated with the threshold photoionization cross-section of the $5s5p\ ^3P_1$ excited state as 10.7 ± 1.7 Mb. The measured values of this Rydberg series are also given in Table 1. The $n^{*3}f$ versus the principal quantum number (n) for the two Rydberg series are plotted in Figure 9. The solid lines are the linear fit to the experimental data points with increasing slopes. The slope of $n^{*3}f$ line for the $5s5p\ ^1P_1 \rightarrow 5snd\ ^1D_2$ series is larger than that of the $5s5p\ ^3P_1 \rightarrow 5snd\ ^3D_2$ Rydberg series, a clear indication of configuration interactions.

Table 1. Oscillator strengths data corresponding to the $5s5p\ ^1P_1 \rightarrow 5snd\ ^1D_2$ and $5s5p\ ^3P_1 \rightarrow 5snd\ ^3D_2$ Rydberg transitions.

n	$5s5p\ ^1P_1 \rightarrow 5snd\ ^1D_2$			$5s5p\ ^3P_1 \rightarrow 5snd\ ^3D_2$	
	Wavelength (nm)	Oscillator Strength Present Work	Mende and Kock [18]	Wavelength (nm)	Oscillator Strength
20	418.66	1.7E-3			
21	418.03	1.5E-3			
22	417.50	1.4E-3			
23	417.04	1.3E-3			
24	416.65	1.2E-3		320.63	2.4E-5
25	416.30	1.1E-3		320.42	2.1E-5
26	416.00	1.1E-3		320.23	1.9E-5
27	415.73	1.1E-3		320.07	1.8E-5
28	415.50	8.7E-4		319.92	1.8E-5
29	415.29	8.0E-4		319.80	1.6E-5
30	415.10	7.8E-4	6.8E-4	319.68	1.5E-5
31	414.93	7.0E-4	6.0E-4	319.58	1.3E-5
32	414.78	5.5E-4	5.6E-4	319.48	1.1E-5
33	414.64	4.9E-4	4.9E-4	319.40	1.1E-5
34	414.52	4.7E-4	4.4E-4	319.32	9.9E-6
35	414.41	4.3E-4	4.8E-4	319.25	9.8E-6
36	414.30	4.6E-4	4.2E-4	319.19	8.5E-6
37	414.21	3.9E-4	4.1E-4	319.13	8.7E-6
38	414.12	3.9E-4	4.0E-4	319.08	7.2E-6
39	414.04	3.4E-4	3.6E-4	319.03	7.5E-6
40	413.97	3.5E-4	3.5E-4	318.99	7.1E-6
41	413.90	2.9E-4	3.3E-4	318.95	6.4E-6
42	413.84	3.2E-4	3.4E-4	318.91	5.8E-6
43	413.78	3.4E-4	3.0E-4	318.87	5.2E-6
44	413.73	2.6E-4	2.8E-4	318.84	5.5E-6
45	413.68	2.6E-4	2.7E-4	318.81	5.4E-6
46	413.63	2.3E-4	2.4E-4	318.78	4.8E-6
47	413.59	2.3E-4	2.5E-4	318.76	4.6E-6
48	413.54	2.1E-4	2.5E-4	318.73	4.0E-6
49	413.51	1.8E-4	2.2E-4	318.71	4.4E-6
50	413.47	1.9E-4	2.0E-4	318.69	3.3E-6
51	413.44	1.7E-4	2.1E-4	318.67	4.1E-6
52	413.41	1.6E-4	1.9E-4	318.65	3.7E-6
53	413.38	1.8E-4	1.8E-4	318.63	3.4E-6
54	413.35	1.8E-4	1.7E-4	318.61	3.4E-6
55	413.32	1.5E-4	1.6E-4	318.60	2.4E-6
56	413.30	1.6E-4	1.6E-4	318.58	2.9E-6
57	413.27	1.3E-4	1.3E-4	318.57	2.7E-6
58	413.25	1.3E-4	1.3E-4	318.55	2.9E-6
59	413.23	1.2E-4	1.2E-4	318.54	2.2E-6
60	413.21	1.1E-4	1.0E-4	318.53	1.9E-6
61	413.19	1.1E-4		318.52	2.4E-6
62	413.17	1.0E-4		318.51	2.1E-6
63	413.15	9.9E-5		318.50	2.2E-6
64	413.14	9.2E-5		318.49	2.1E-6
65	413.12	8.7E-5		318.48	2.0E-6
66	413.11	8.4E-5		318.47	2.0E-6
67	413.09	8.2E-5		318.46	1.8E-6
68	413.08	7.7E-5		318.45	1.7E-6
69				318.44	1.9E-6
70				318.43	1.7E-6

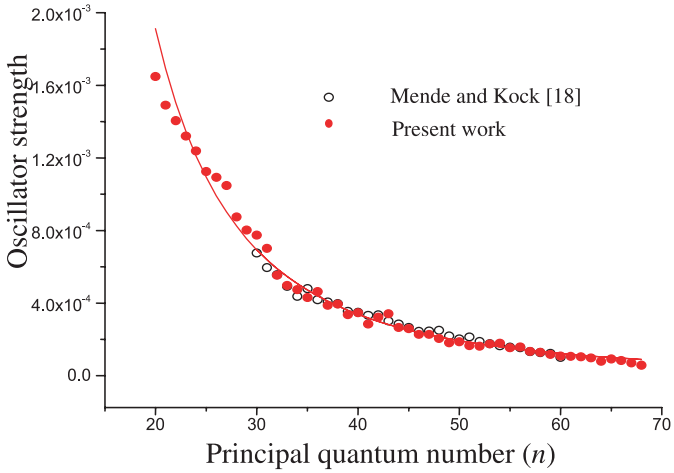

Fig. 8. A plot of the oscillator strengths of the $5s5p\ ^1P_1 \rightarrow 5snd\ ^1D_2$ ($19 \leqslant n \leqslant 68$) Rydberg series versus the principal quantum number (n). The hollow circular data points are that of Mende and Kock [18] and the solid circular data points are from the present work.

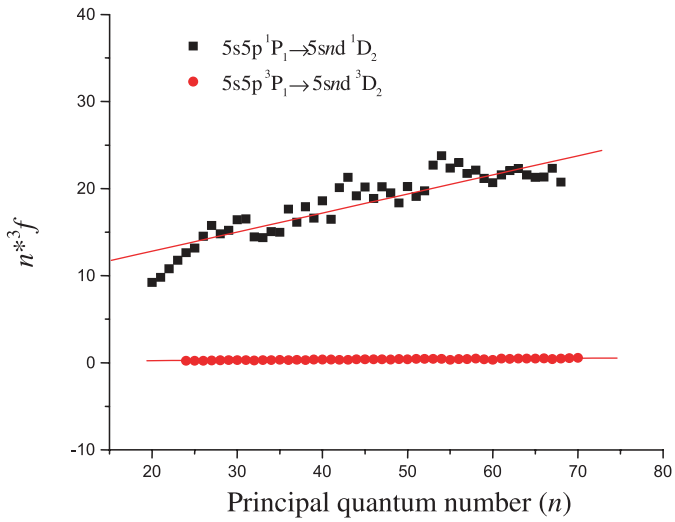

Fig. 9. Plot of the $(n*)^3 f$ versus the principal quantum number (n) corresponding to the $5s5p\ ^1P_1 \rightarrow 5snd\ ^1D_2$ ($19 \leqslant n \leqslant 68$) and the $5s5p\ ^3P_1 \rightarrow 5snd\ ^3D_2$ ($24 \leqslant n \leqslant 70$) Rydberg transitions of strontium.

In the next step we have extended our studies from the discrete region to the above threshold ionization region. The oscillator strengths (f-values) in the discrete region is related to the differential oscillator strengths in the above threshold region as [41]

$$\frac{(n^*)^3 f}{2R} = \frac{df}{dE} \tag{6}$$

where n^* is the effective quantum number, f is the oscillator strength of the discrete transition, R is the Rydberg constant and E is the photon energy of the transition connecting the excited state and the continuum. The oscillator strengths distribution in the continuum is also related

Table 2. Experimental data for the absolute photoionization cross section from the $5s5p\ ^3P_1$ excited state of strontium.

state	Present work wavelength (nm)	cross section (Mb)	$\left(\frac{df}{dE}\right)_E$ (eV^{-1})	Previous work cross section (Mb)
$5s5p\ ^3P_1$	318.2	10.7 ± 1.7	0.097	
	317	11.2 ± 1.8	0.102	
	315	10.6 ± 1.7	0.096	
	313	9.2 ± 1.5	0.084	
	310	7.2 ± 1.1	0.066	
	266	2.4 ± 0.4	0.022	2.3 [40]

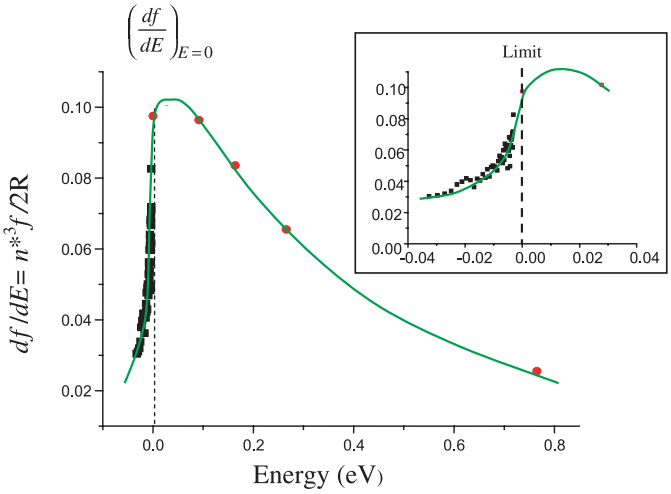

Fig. 10. The experimentally measured distribution of the oscillator strengths in the discrete and in the continuum region corresponding to the $5s5p\ ^3P_1 \rightarrow 5snd\ ^3D_2$ Rydberg series of strontium.

to the photoionization cross-section as [41]

$$\frac{df}{dE} = 9.11 \times 10^{15}\sigma(E). \quad (7)$$

The $5s5p\ ^3P_1 \rightarrow 5snd\ ^3D_2$ Rydberg series have been observed up to much higher principal quantum number ($n = 70$) therefore we have selected this series to determine the behavior of the distribution of the oscillator strength in the continuum region.

The differential oscillator strengths for six different regions of the continuum were then calculated from the measured values of the photoionization cross sections corresponding to the $5s5p\ ^3P_1$ excited state using equation (7). The calculated values of differential oscillator strengths at the excess energies of 0 eV, 0.014 eV, 0.035 eV, 0.064 eV, 0.103 eV and 0.764 eV at and above the first ionization threshold are given in Table 2. In order to give an overall view of the oscillator strength distribution from the $5s5p\ ^3P_1$ excited state of strontium, we have plotted the discrete f-values and the corresponding oscillator strength density df/dE in the continuum on the same graph in Figure 10. The solid line is a freehand sketch to the experimental data points just to show the trend of the oscillator strength distribution in the discrete and continuum regions while the dashed line represents the ionization threshold. Figure 10 clearly indicates a smooth merging of the discrete absorption features into the continuous absorption across the ionization threshold for the $5s5p\ ^3P_1 \rightarrow 5snd\ ^3D_2$ Rydberg series. The inset in the figure shows an expanded view of the discrete region and near the threshold ionization continuum from -0.04 eV to 0.04 eV. This kind of connection up to and beyond the ionization threshold was discussed by Berkowitz [41] and Fano and Cooper [1].

The maximum overall uncertainty in the determination of the absolute photoionization cross section is estimated to be ≈15%, which is attributed to the experimental errors in the measurements of the laser energy, the cross sectional area of the laser beam at the focusing volume, the calibration of the detection system and a non-uniform transmission of the quartz windows. The f-values are quoted ≈18% uncertainty, which is due to an additional uncertainty in measurement of the transition energy and integrated line intensities.

In conclusion we have reported the oscillator strengths for the $5s5p\ ^1P_1 \rightarrow 5snd\ ^1D_2$ and $5s5p\ ^3P_1 \rightarrow 5snd\ ^3D_2$ Rydberg series of strontium using the threshold values of the photoionization cross sections from the two excited states of strontium. The measurements were extended to the ionization continuum for the $5s5p\ ^3P_1 \rightarrow 5snd\ ^3D_2$ Rydberg transitions and a smooth connection between the discrete f-values and the oscillator strengths distribution in the continuum has been established. This technique can be extended to determine the oscillator strength distribution in the discrete and the continuous spectra of all the alkali and the alkaline earth elements. Further work in this direction is in progress in our laboratory.

We are greatful to Professor M. Kock, Hannover University, Germany for clarifying some points relating to the measurements of the oscillator strengths of Rydberg transitions of alkaline earth metals. The present work was financially supported by the Higher Education Commission (HEC), Pakistan Science Foundation, and the Quaid-I-Azam University, Islamabad, Pakistan. Sami-ul-Haq, M. Rafiq and M A Kalyar are grateful to the HEC for the grant of Ph.D. scholarship under the Indegenous scheme.

References

1. U. Fano, J.W. Cooper, Rev. Mod. Phys. **40**, 441 (1968)
2. G.W.F. Drake, *Handbook of Atomic, Molecular, & Optical Physics* (Springer, Berlin, 2006)
3. M.C.E. Huber, R.J. Sandeman, Rep. Prog. Phys. **49**, 397 (1986)
4. P. Ewart, A.F. Purdie, J. Phys. B: At. Mol. Phys. **9**, L437 (1976)
5. P. Esherick, Phys. Rev. A **15**, 1920 (1977)
6. J.R. Rubbmark, S.A. Borgstrom, Phys. Scripta **18**, 196 (1978)
7. R. Beigang, K. Lücke, A. Timmermann, P.J. West, Opt. Commun. **42**, 19 (1982)

8. R. Beigang, K. Lücke, D. Schmidt, A. Timmermann, P.J. West, Phys. Scripta **26**, 183 (1982)
9. C.J. Dai, Phys. Rev. A **52**, 4416 (1995)
10. M.A. Baig, M. Yaseen, Ali Raheel, Nadeem Ali, S.A. Bhatti, Eur. Phys. J. D **6**, 201 (1999)
11. Y. Makdisi, G. Philip, K.S. Bhatia, J.P. Connerade, J. Phys. B: At. Mol. Phys. **34**, 521 (2001)
12. W. Wiese, *Progress in Atomic Spectroscopy*, edited by W. Hanle, H. Kleinpoppen (Plenum, New York, 1979), Part B 1101
13. C. Barrientos, I. Martin, Can. J. Phys. **65**, 435 (1987)
14. C. Barrientos, I. Martin, Can. J. Phys. **66**, 29 (1988)
15. H.G.C. Werij, H. Chirs, C.E. Green, Theodosiou, A. Gallagher, Phys. Rev. A **46**, 1248 (1992)
16. W.H. Parkinson, E.M. Reeves, F.S. Tomkins, J. Phys. B: At. Mol. Phys. **9**, 157 (1976)
17. W.R.S. Garton, J.P. Connerade M.A. Baig, J. Hormes, B. Alexa, J. Phys. B: At. Mol. Phys. **16**, 389 (1983)
18. W. Mende, M. Kock, J. Phys. B: At. Mol. Opt. Phys. **29**, 655 (1996)
19. C.E. Burkhardt, J.L. Libbert, Xu Jian, J.J. Leventhal, J.D. Kelley, Phys. Rev. A **38**, 5949 (1988)
20. L.W. He, C.E. Burkhardt, M. Ciocca, J.J. Leventhal, Phys. Rev. Lett. **67**, 2131 (1991)
21. W. Mende, K. Bartschat, M. Kock, J. Phys. B: At. Mol. Opt. Phys. **28**, 2385 (1995)
22. U. Griesmann, B. Esser M.A. Baig, J. Phys. B: At. Mol. Opt. Phys. **25**, 3475 (1992)
23. K. Niemax, Appl. Phys. B. **38**, 147 (1985)
24. R.E. Honig, D.A. Kramer,Vapor Pressure Data for Solids and Liquid Elements RCA Review **30**, 285 (1969)
25. D. Hanna, P.A. Karkainen, R. Wyatt, Opt. Quantum Electron. **7**, 115 (1975)
26. NIST Database, `www.phys.nist.gov` (2006)
27. N. Amin, S. Mahmood, M. Anwar-ul-Haq, M. Riaz, M.A. Baig, Eur. Phys. J. D **37**, 23 (2006)
28. S. Mahmood, N. Amin, Sami-ul-Haq, N.M. Shaikh, S. Hussain, M.A. Baig, J. Phys. B: At. Mol. Opt. Phys. **39**, 2299 (2006)
29. S. Hussain, M. Saleem, M. Rafiq, M.A. Baig, Phys. Rev. A **74**, 022715 (2006)
30. S. Hussain, M. Saleem, M.A. Baig, Phys. Rev. A **74**, 052705 (2006)
31. M. Saleem, S. Hussain, M. Rafiq, M.A. Baig, J. Phys. B: At. Mol. Phys. **39**, 5025 (2006)
32. W. Demtröder, *Laser Spectroscopy* (Springer, Berlin, 1996)
33. J.M. Song, T. Inoue, H. Kawazumi, T. Ogawa, Anal. Sci. **15**, 601 (1999)
34. V. Svedas, J. Phys. B: At. Mol. Opt. Phys. **21**, 301 (1988).
35. J.T. Manson, S.T. Manson, Phys. Rev. A **43**, 4684 (1991)
36. W. Mende, M. Kock, J. Phys. B: At. Mol. Opt. Phys. **30**, 5401 (1997)
37. T.S. Yih, H.H. Wu, C.C. Chu, H.S. Fung, Y.P. Lin, S.J. Hsu, J. Korean Phys. Soc. **32**, 405 (1998)
38. C.C. Chu, H.S. Fung, H.H. Wu, T.S. Yih, J. Phys. B: At. Mol. Phys. **31**, 3843 (1998)
39. M. Martin, W.H. Hugo, J. Phys. B: At. Mol. Opt. Phys. **38**, 1895 (2005)
40. O.R. Jones, R.M. Perks, H.H. Telle, Rap. Comm. Mass Spectrom. **10**, 1725 (1996)
41. J. Berkowitz, *Photoabsorption, Photoionization and Photoelectron Spectroscopy* (Academic Press, New York, 1979)
42. C.E. Moore, *Atomic Energy Levels* (NSRDS-NBS, 1971), Vol. II